ACS OMEGA

http://pubs.acs.org/journal/acsodf

Article

Mechanism and Practice of Multifracturing Using Dynamic Loads in a Low-Permeability Coal Reservoir

Yufei Qi, Lin Tian,* Yunxing Cao, Jinghao Wu, Junsheng Zhang, Yongxing Cao, and Baoku Cui

Cite This: *ACS Omega* 2023, 8, 6584−6596

Read Online

ACCESS | Metrics & More | Article Recommendations

ABSTRACT: The geological conditions of coal reservoirs in China are complex, and the reservoir permeability is generally lower. Multifracturing is an effective method of improving reservoir permeability and coalbed methane (CBM) production. In this study, two types of dynamic loads, CO_2 blasting and a pulse fracturing gun (PF-GUN), were used to conduct multifracturing engineering tests in nine surface CBM wells in the Lu'an mining area in the central and eastern parts of the Qinshui Basin. The curves of pressure versus time of the two dynamic loads were obtained in the laboratory. The prepeak pressurization time of the PF-GUN was 200 ms, and that of the CO_2 blasting was 2.05 ms, which just falls in the optimum pressurization time of multifracturing. The microseismic monitoring results revealed that, in terms of the fracture morphology, both the CO_2 blasting and PF-GUN loads produced multiple sets of fractures in the near-well zone. In the six wells used for the CO_2 blasting tests, an average of three branch fractures were produced outside of the main fracture, and the average angle between the main fracture and the branch fractures exceeded 60°. In the three wells stimulated by PF-GUN, an average of two branch fractures were produced outside of the main fracture, and the average angle between the main fracture and the branch fractures was 25−35°. The multifracture characteristics of the fractures formed via CO_2 blasting were more obvious. However, a coal seam is a multifracture reservoir with a large filtration coefficient; the fracture will not extend after reaching the maximum scale under a certain gas displacement condition. Compared with the traditional hydraulic fracturing technique, the nine wells used in the multifracturing tests exhibited an obvious stimulation effect with an average increase of 51.4% in daily production. The results of this study provide an important technical reference for the efficient development of CBM in low- and ultralow-permeability reservoirs.

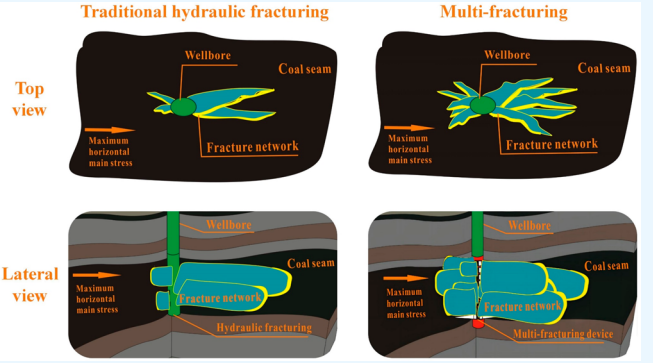

1. INTRODUCTION

For low-permeability reservoirs, increasing the permeability is the key to improving coalbed methane (CBM) production.[1−3] Network fracturing has achieved great success in the development of shale gas in extremely low permeability reservoirs,[4,5] which has important reference significance for the development of CBM. The core of network fracturing technology is a horizontal well and multistage fracturing.[6−8] The basic theory is to use multistage fracturing to form stress interference in the reservoir.[9−11] Through bending and expansion of the fractures formed via fracturing, the primary fractures in the reservoir are connected to the maximum extent possible, thus increasing the permeability and conductivity of the reservoir. The purpose of multifracturing is to form multiple main radial fractures around the wellbore and then to extend microfractures from the multiple main fractures.[12,13]

The similarity between the multifracturing technique and the network fracturing technique is that both make full use of natural weak structural surfaces such as natural fractures and rock bedding.[13] The goal is to increase the multilevel secondary microfractures around the artificial main fractures and finally to form a fracture system in which the artificial main fractures, natural weak structural surfaces, and multilevel secondary microfractures interweave and communicate with each other.[14,15] However, there are also fundamental differences between the multifracturing and network fracturing methods. Network fracturing aims to open up the connectivity of the cleats and form curved and coiled microfractures around the main fractures. In addition to the tensile failure of the bedrock, the fractures produced by multifracturing also include the mechanical behaviors of natural fractures, such as shearing, sliding, and staggering.[16,17] High-density fracture behavior

Received: October 31, 2022
Accepted: January 31, 2023
Published: February 9, 2023

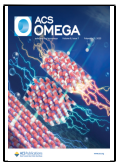

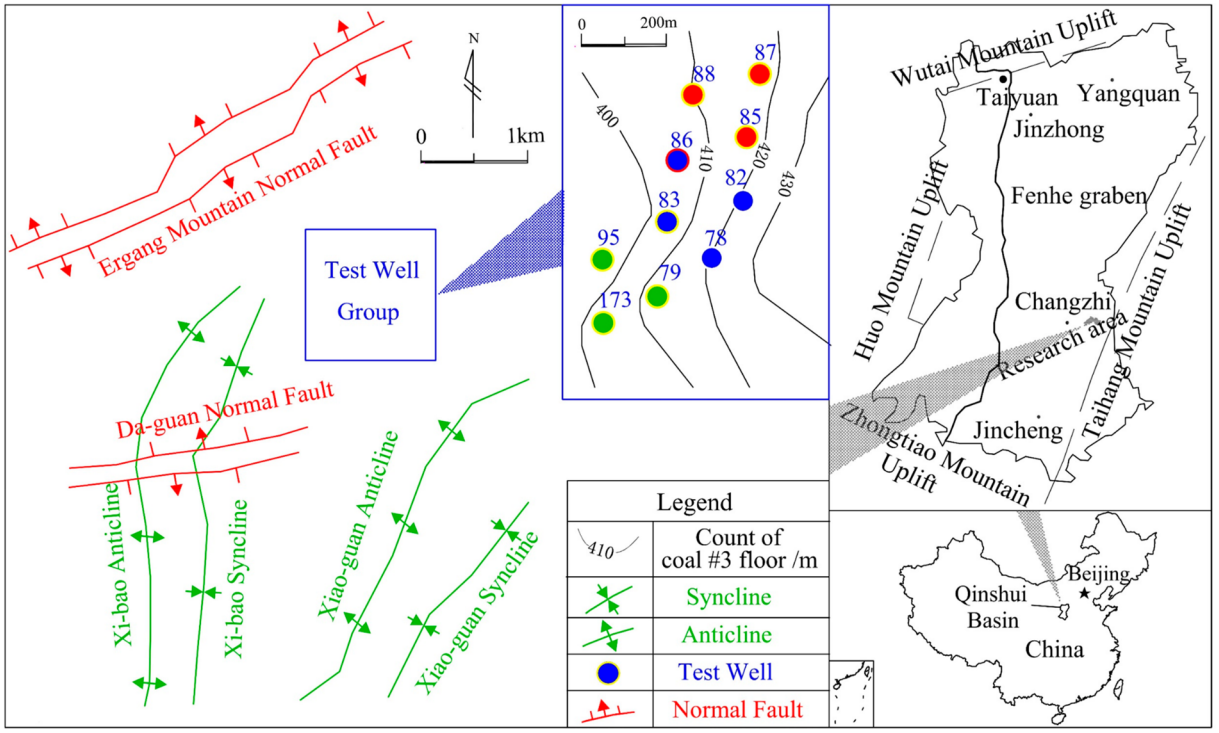

Figure 1. Structural diagram of the Gaohe mine field. The study area is located in the southeast of Qinshui Basin, China, and the 10 testing wells, labeled HG78, HG79, HG82, HG83, HG85, HG86, HG87, HG88, HG95, and HG173 are distributed in an area of about 1.2 km^2.

alleviates the stress concentration in the coal and rock mass and homogenizes the in situ stress state within the influence range of the fracturing. In addition, it guides the formation of the multifracturing effect over a wider range and it increases the conductivity of the fractures at the same scale. It can be said that multifracturing is an enhanced version of network fracturing.[18]

Multifracturing has been studied for a long time in conventional oil, gas, and shale gas development,[19−21] but there is no precedent for its application to CBM production. In conventional oil and gas development, multifracturing is mainly based on high-energy gas fracturing.[22,23] In this process, a rocket propellant produces in situ stress pulses in a short time at the target layer,[24] increasing the stimulated reservoir volume (SRV) by generating multiple radial fractures with stress pulses[25] and thereby fracturing the stratum and increasing production and injection. The pressure pulse generated by the thermochemical fracturing method generates a large number of complex microfractures, which leads to the reduction of breakdown pressure and breakdown time and more effectively guides the design and production of a subsequent hydraulic fracturing treatment.[26−31] However, compared with conventional oil and gas sandstone reservoirs, coal reservoirs have a smaller elastic modulus and larger Poisson ratio, making them typical incompressible or difficult-to-compress reservoirs in conventional oil and gas reservoirs. To achieve the radial expansion effect of multifracturing in coal reservoirs, the performance of the fracturing load must be optimized based on the geomechanical characteristics of coal reservoirs.

CO_2 blasting is a green fracturing technology, has less impact on the formation and environment, and has the potential of mitigating global warming.[32] CO_2 blasting is a dynamic load fracturing technique, which involves the conversion of liquid CO_2 into the gas phase to release a large amount of energy into the coal rock, thus producing a fracturing effect.[33−36] Compared with high-energy gas fracturing, the dynamic load formed by CO_2 blasting has a lower frequency and longer wavelength, which can form a large fracture system in coal reservoir. CO_2 blasting has been shown to have great technical advantages in underground gas drainage in coal mines.[37,38] The influence radius of a single hole reaches 7−12 m,[39] the permeability of the reservoir increases by 50−100 times on average, and the flow rate of the single-hole gas extraction increases by 2−8 times.[40] Unfortunately, this method has not been tested and applied in surface CBM wells.

In this study, a set of multifracturing experiments for CBM production were conducted in Lu'an mining area in the central and eastern parts of the Qinshui Basin, Shanxi Province, China. Two methods were used in the experiments, CO_2 blasting and pulse fracturing gun (PF-GUN). Based on the two groups of experimental results, the fracture distribution pattern and the effect on increasing the CBM production after fracturing were analyzed in detail, and the advantages of CO_2 blasting in multifracturing were determined. The results of this study have important significance for promoting the efficient development of CBM in ultralow-permeability coal reservoirs.

2. ENGINEERING EXPERIMENTS AND METHODS

2.1. Geologic Setting. From 2017 to 2018, a set of multifracturing engineering tests were completed in the Lu'an mining area, the central section of the eastern margin of the Qinshui Basin, Shanxi Province, China. The tests were conducted in 10 test wells. CO_2 blasting was conducted in six wells, PF-GUN was conducted in three wells, and one well was used as a comparison well.

The test well group was located in the northern part of the Gaohe mine field in the Lu'an group. The control area of the

https://doi.org/10.1021/acsomega.2c07001
ACS Omega 2023, 8, 6584−6596

Table 1. Statistics of the Completion Parameters of the 10 Test Wells

well no.	burial depth (m)	floor elevation (m)	coal seam thickness (m)	reservoir stress (MPa)	reservoir stress gradient (MPa/100 m)	permeability (mD)
HG 78	493.2	422.09	6.25	2.42	0.49	
HG 79	507.3	415.82	7.1	2.24	0.44	
HG 82	504.85	422.25	5.3	2.48	0.49	0.45
HG 83	524.74	401.86	6.0	2.79	0.53	
HG 85	512.95	414.77	7.8	2.63	0.51	
HG 86	522.68	405.15	6.65	2.88	0.55	
HG 87	512.17	415.87	7.1	2.17	0.42	
HG 88	517.57	410.32	7.1	2.26	0.44	0.058
HG 95	531.87	393.75	7.1	2.62	0.49	0.083
HG 173	512.6	402.85	6.6	1.62	0.32	
average value	**513.9**	**410.4**	**6.7**	**2.41**	**0.47**	

10 test wells was about 1.2 km^2. There is no obvious geological structure in the area, and the entire area is a monoclinic structure that is high in the east and low in the west (Figure 1). The target stratum for CBM development was the #3 coal seam in the Permian Shanxi Formation. The burial depth was 493.20−531.87 m, with an average of 513.9 m. The floor elevation was 393.75−422.25 m, with an average of 410.4 m. The coal seam thickness was 5.30−7.8 m, with an average of 6.7 m. The coal structure type of the #3 coal seam was mainly primary structure coal and catallactic coal, and the fractures were uneven and conchoidal. The initial reservoir stress was 1.62−2.88 MPa, with an average of 2.41 MPa and a stress gradient of 0.32−0.55 MPa/100 m. The measured permeability of the #3 coal seam was 0.083−0.45 mD, with an average of 0.197 mD, making it a typical low-stress and low-permeability coal reservoir. The basic reservoir parameters are presented in Table 1.

The microseismic monitoring results of several CBM wells in the adjacent area revealed that the horizontal maximum principal stress in the area was 9.15−17 MPa, with an average of 14.25 MPa, and the minimum principal stress was 7.79−10.56 MPa, with an average of 8.83 MPa. The horizontal maximum principal stress direction was NE 36.1−48.5°, and the lateral stress ratio was about 1.61.

2.2. CO_2 Blasting Experiments. In the CO_2 blasting experiment, a type φ89 mm fracturing pipe made by Henan Polytechnic University,[33,38] China, was used. The fracturing pipe consisted of an inflation valve, heater, fracturing tube, controlled-pressure shears, and jet valve. The liquid CO_2 capacity was determined by the length of the reservoir tube, which was an average 1 m reservoir tube containing 3.5 kg of liquid CO_2. The blasting pressure of the fracturing pipe was determined by the thickness of the controlled pressure shears. The greater the thickness of the controlled pressure shears, the higher the blasting pressure. To ensure the stability of the fracturing pipe in the well after blasting, the project design adopted the double pipe hedging operation process: that is, the release head of the No. 1 fracturing pipe was directly connected to the release head of the No. 2 fracturing pipe.

The CO_2 blasting experiment was mainly completed using a crane and logging truck. The steps of the experiment mainly included magnetic positioning depth sounding and bottoming, CO_2 blasting into the well, wellbore liquid injection, fracturing operation, and removal of the equipment from the well; the workflow is shown in Figure 2. A single well generally operated for 2−3 cycles. The relevant test parameters are presented in Table 2.

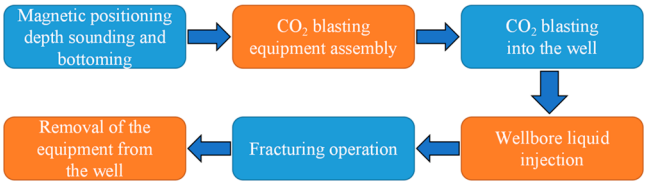

Figure 2. Workflow diagram of CO_2 blasting.

Table 2. Statistics of CO_2 Blasting Test Parameters

well no.	no. of operation cycles	blasting pressure (MPa)	liquid CO_2 capacity (kg)
HG 82	1	45	13.1
HG 85	1	30	14.5
	2	30	21.05
HG 87	1	45	13.6
	2	60	20.2
HG 88	1	30	21.1
	2	45	21.1
	3	30	13.2
HG 83	1	30	27.4
	2	60	20.3
	3	60	13.8
	4	60	13.4
HG 86	1	60	13.2
	2	60	20.3
	3	60	21.1
	4	60	27.2

2.3. PF-GUN Experiments. The PF-GUN is a new type of high-energy gas fracturing technology.[41,42] It uses propellants with different burning rates as the power source. Through optimization of the design of the charge structure, the pressure rise time, pressure peak, and pressure action process can be accurately controlled. A multistage gas stratum can be fractured at the same time to produce multiple fractures and to communicate with the natural fractures in the coal seam to increase production.[43]

The operation process of the PF-GUN was the same as that used forCO_2 blasting (Figure. 3). The PF-GUN has no postcombustion residue and the equipment can be reused. And the workflow of PF-GUN is shown in Figure 4. The PF-GUN technique was used in test three wells, such as well HG 95. The relevant test parameters are presented in Table 3.

2.4. Testing the Multifracturing Effect. Microseismic monitoring is a geophysical technique in which acoustic emissions and seismic activity are used to monitor the

https://doi.org/10.1021/acsomega.2c07001
ACS Omega 2023, 8, 6584−6596

Figure 3. PF-GUN operation site. After the PF-GUN operation, the wellbore water column rushed out about 22 m due to a sudden pressure increase in the bottom hole.

influence, effect, and reservoir state by observing and analyzing microseismic events generated during production activities.[44−46] In recent years, the theoretical method of microseismic monitoring has been rapidly developed.[47,48] Because of its advantages in verifying and modifying fracturing models,[49] guiding the selection of the fracturing fluid and judging the amount of sand, ensuring the fracturing operation according to the design, improving the production after fracturing, and extending the validity period after fracturing,[50] it has gradually attracted widespread attention. The morphology of the fractures created via fracturing is an important index used to evaluate the fracturing effect. The distribution of the fracture morphology includes parameters such as the number of fractures and the fracture intersection angle.

The entire fracturing process in the 10 multifractured wells was monitored using the microseismic monitoring method. The fracturing monitoring stations were deployed in a star pattern, with the wellhead as the center and a radius of 60−120 m (Figure 5). First, 30 min of debugging was conducted before the start of the fracturing preparation; after the completion of the fracturing, the monitoring was continued for 30 min to ensure the integrity of the data received.

3. RESULTS AND DISCUSSION

3.1. Fracture Morphology Produced via Multifracturing. The ground microseismic monitoring method was used to monitor the entire process during the two groups of tests. Based on an inversion of the source information, the fracture morphology and influence radius of the two preset reservoir fracturing techniques were determined.

3.1.1. Influence Radius of Fracturing. The influence radius of the fracturing is an important parameter for measuring the fracturing effect. The influence radii of the fracturing in the two groups of tests are presented in Table 4. The influence radius of the CO_2 blasting was 16.3−29.9 m, and the influence radius

Table 3. Statistics of the PF-GUN Test Parameters[a]

well no.	no. of operation cycles	PF-GUN capacity (kg)
HG 95	1	11.4
	2	11.4
HG 173	1	11.4
	2	11.4
HG 79	1	11.4
	2	11.4

[a]Type φ89 mm, outer diameter of 60 mm, density of 3.8 kg/m^3. Gas production of 960 L/kg at 10 °C and 101 kPa.

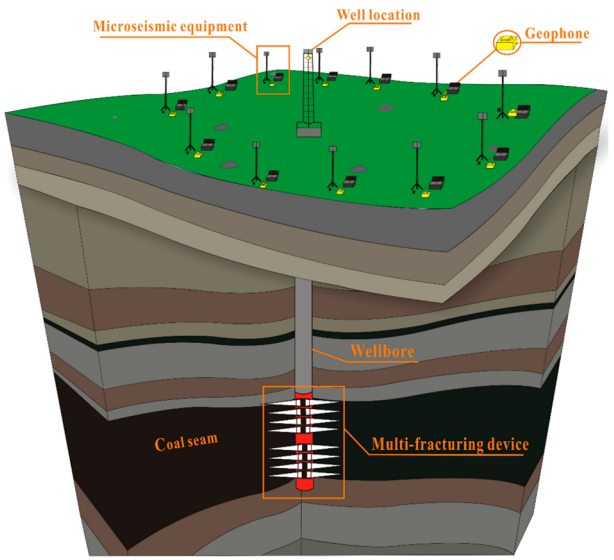

Figure 5. Monitoring station layout. 12 geophones were arranged in a circular area of about 150 m range around the wellhead. The changes of fractures in the coal reservoir were analyzed by a subsequent processing.

of the PF-GUN was 18.5−37.6 m; the PF-GUN-induced radial fracture length is better than that of CO_2 blasting.

3.1.2. Fracture Morphology Distribution. The fracture morphology produced via fracturing is an important index for evaluating the fracturing effect. The distribution of the fracture morphology includes the number of fractures and the fracture intersection angle. To more clearly explain the fracture morphology characteristics of the multifractures produced via the fracturing methods, the monitoring results of well HG 79 (PF-GUN test) and well HG 83 (CO_2 blasting test) were selected for illustration.

3.1.2.1. Fracture Morphology Distribution of Well HG 83 for CO_2 Blasting Test. From a top view of the effective events recorded via microseismic monitoring, it can be seen that the fracture morphology formed using the CO_2 blasting technique in well HG 83 is asymmetrically crossed, and the influence radius is 21.3−24.6 m (Figure 6a). The overall shape of the fracture is not obviously controlled by the direction of the regional principal stress. The main fracture (blue) produced by fracturing is oriented NE60°, and there are three obvious

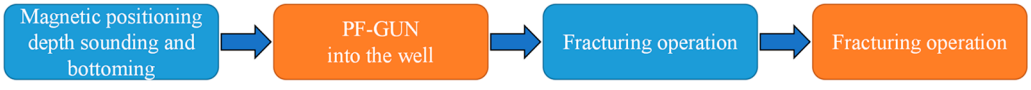

Figure 4. Workflow diagram of PF-GUN.

https://doi.org/10.1021/acsomega.2c07001
ACS Omega 2023, 8, 6584−6596

Table 4. Statistics of the Microseismic Monitoring Parameters

technique	well number	no. of operation cycles	influence radius (m)	no. of effective microseismic events	standard error
CO_2 blasting	HG 82	1	16.3−20.6	20	1.5399
	HG 83	4	21.3−24.6	20	
	HG 85	2	23.1−29.2	18	
	HG 86	4	19.6−23.3	14	
	HG 87	2	25.7−29.9	22	
	HG 88	3	26.2−28.7	18	
PF-GUN	HG 95	2	27.3−29.6	21	4.6767
	HG 173	2	18.5−21.4	16	
	HG 79	2	37.0−37.6	28	

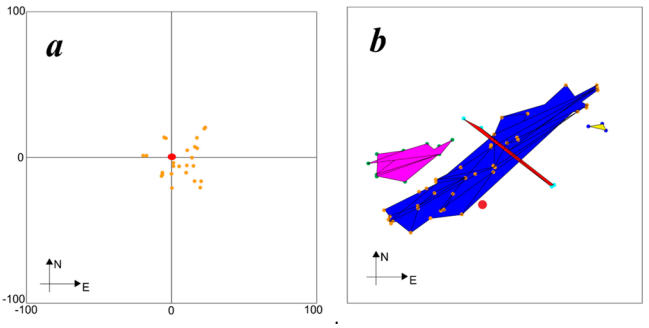

Figure 6. Top view of microseismic events and three-dimensional fractures formed via CO_2 blasting in well HG 83. The yellow dots in (a) represent microseismic events, and the colored lines in (b) represent a potential fracture network. The larger blue networks indicate the primary fracture, while the purple, red, and yellow networks represent the branch fractures.

branch fractures, which are oriented NE80°, NW59°, and nearly east−west. The intersection angle of the four main fractures is 119°, and they exhibit typical multifracture characteristics (Figure 6b). According to the microseismic results of other wells, the number of fractures after CO_2 blasting is 4−5.

Figure 7 shows the development state of the primary fractures in the near-well area induced by CO_2 blasting in well

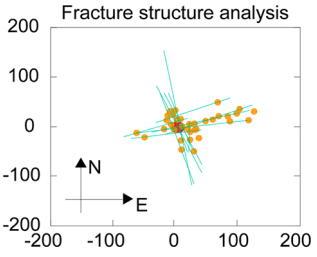

Figure 7. Trend of original fractures induced by CO_2 blasting. The yellow dots represent the microseismic events, and the green lines indicate the direction and scale of original fractures induced by CO_2 blasting.

HG 83. The induced fractures were divided into two groups, NE 50−70° and NW 20−40°, which were crossed. The angle between the directions of the radial fractures induced by CO_2 blasting is approximately vertical, making it easier for later hydraulic fracturing to expand around the wellbore and increasing the stimulated reservoir volume (SRV).

3.1.2.2. Fracture Distribution Morphology of Well HG 79 in PF-GUN Test. It can be seen from the top view of the effective events recorded via microseismic monitoring that the fractures formed using the PF-GUN technique in well HG 79 are elliptical in shape with an influence radius of 37.0−37.6 m (Figure 8a), and the overall shape of the fractures is controlled

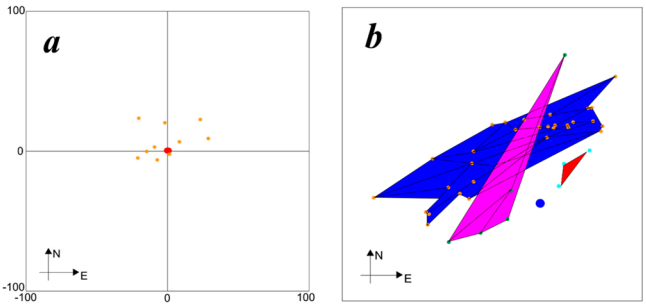

Figure 8. Top view of microseismic events and three-dimensional fractures produced via PF-GUN in well HG 79. The yellow dots in (a) represent microseismic events, and the colored lines in (b) represent a potential fracture network. The larger blue networks indicate the primary fracture, while the purple and red networks represent the branch fractures.

by the direction of the regional principal stress. The main fracture (blue) produced via fracturing is oriented NE60°, and there are two obvious branch fractures, which are oriented NE25° and NE40° (Figure 8b). Compared with the CO_2 blasting technique, after the PF-GUN technique was applied, there was no obvious sign of fracture extension in the coal reservoir outside the direction of the regional maximum principal stress, but the influence radius of the PF-GUN technique was relatively large.

Figure 9 shows the development state of the primary fractures in the near-well induced using the PF-GUN technique in well HG 79. The induced fractures were divided into two groups: NE50−70° and NW20−40°. The NE50−70° fractures, which extended along the direction of the maximum principal stress, accounted for a significant proportion of the fractures. This phenomenon also shows that PF-GUN can induce large-scale and dense fractures in a fixed direction, but the fractures formed in other directions are short and few, which has certain limitations for an increase in SRV in later hydraulic fracturing.

3.2. Effect of Multifracturing Stimulation. *3.2.1. Effect of Multifracturing on Fracture Extension.* The influence radius of the fractures formed by the dynamic load was small, and its role in the entire fracturing process was equivalent to presetting a fracture near the wellbore. In this test, after two types of dynamic loads were applied, large-scale hydraulic fracturing was carried out in the 10 test wells. In the processing of the microseismic monitoring results, the time-sharing fracture processing technique was used to restore the dynamic

https://doi.org/10.1021/acsomega.2c07001
ACS Omega 2023, 8, 6584−6596

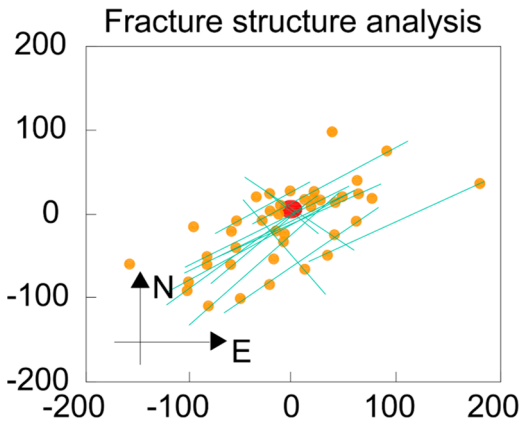

Figure 9. Microseismic monitoring of the trend of the original fissure induced via the PF-GUN technique. The yellow dots represent the microseismic events, and the green lines indicate the direction and scale of original fractures induced by PF-GUN.

process of the fracture propagation. The fracture monitoring results for wells HG 83 and HG 79 were also used to investigate the guiding effect of the dynamic load preset fracture on the extension of the hydraulic fractures.

The fractures produced via conventional hydraulic fracturing generally expand along the direction of the maximum horizontal principal stress,[51−55] and the direction of the fractures is singular. In the case of a preset fracture, hydraulic fracturing can further expand the length of the fracture extension and increase the influence range of the fracturing. It can be seen from the time-division fracture distribution map for well HG 83 (CO_2 blasting fracture presetting) that, after large-scale hydraulic fracturing was conducted, the influence radius reached about 250 m, and the direction of the fracture significantly changed after 65 m, from the original overall EN extension direction to NNE. Through an analysis of the fracture structure, it was found that the fracture scale of the NE fractures was obviously larger than that of the NW fractures. The fractures produced in the first 40 min were oriented NNW; after 60 min, the fractures with this orientation did not expand significantly. After the disturbance of the CO_2 blasting, the hydraulic fractures in well HG 83 first expanded radially around the wellbore and then turned toward the original direction of the ground stress (Figure 10).

It can be seen from the time-division fracture distribution chart for well HG 79 (PF-GUN fracture presetting) that, overall, the subsequent fractures produced via hydraulic fracturing expanded along the direction of the maximum principal stress in the region. Although the NW-trending fractures formed after 20 min, their overall expansion was not obvious, and finally, a dense fracture cluster dominated by NE-trending fractures was formed (Figure 11).

Therefore, the phenomenon that hydraulic fracturing accommodates the original maximum principal stress direction after CO_2 blasting fracture presetting was not obvious. The fracture propagation length was short, and the shape was complex, with a typical crossed fracture pattern. The density of the final fracture network system was almost equal in the NE and NW directions. From the time-division map for the multifracture fracturing, it can be seen that the fracturing fractures in the direction of the nonmaximum principal stress appeared in the initial stage of the fracturing. This phenomenon reflects the guiding effect of the preset fractures on the in situ stress and on the fracturing fractures in the near-wellbore area. The impact load changed the in situ stress in the near-wellbore area and affected the fracture steering.

Table 5 gives the overall fracture orientation, length, and number of branch fractures after hydraulic fracturing in the 10

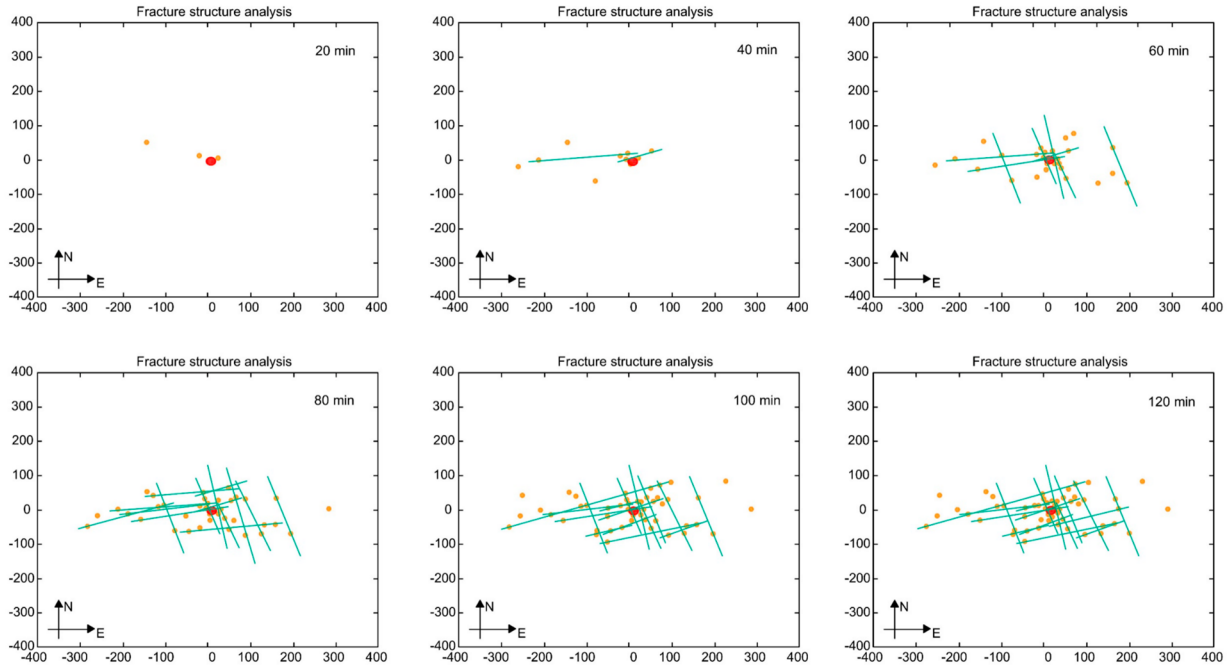

Figure 10. Time slice of the fracture network induced by CO_2 blasting. The fractures formed by CO_2 blasting have an obvious guiding effect on the fracture extension of hydraulic fracturing. The fractures formed within 120 min of hydraulic fracturing are sliced according to time series, and the slice time is marked on the upper right corner of each panel. The yellow dots represent the microseismic events, and the green lines indicate the direction and scale of fractures. It is clear that the fracture scale and influence area increase gradually over time.

https://doi.org/10.1021/acsomega.2c07001
ACS Omega 2023, 8, 6584−6596

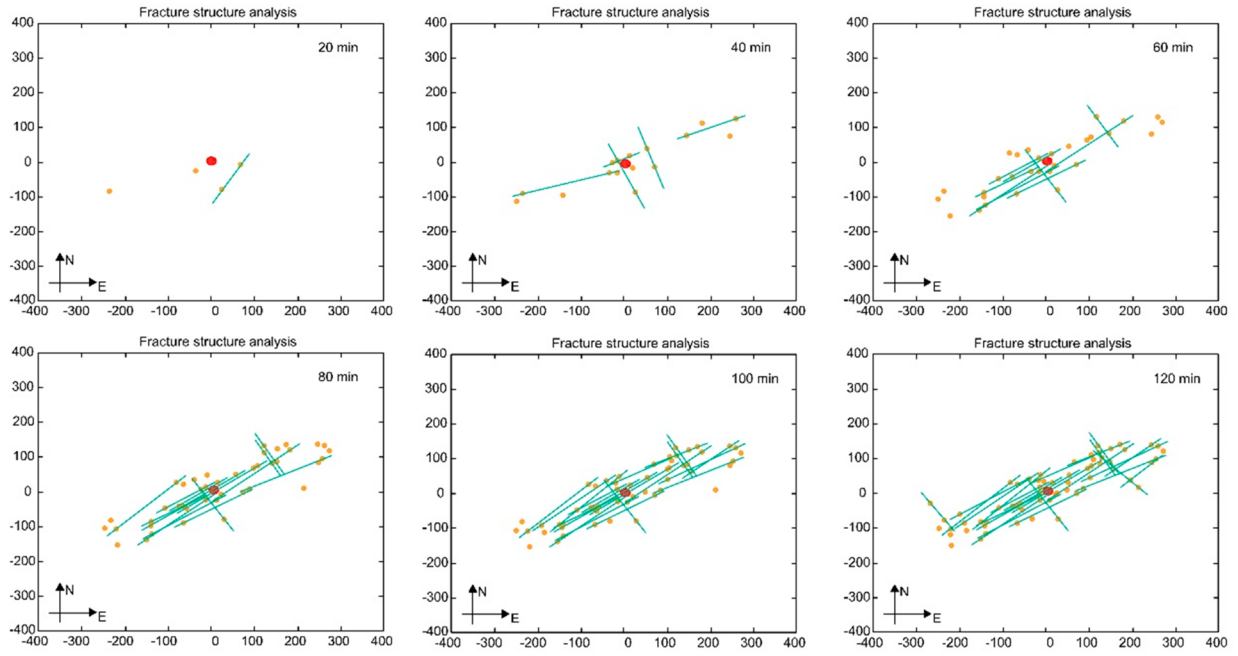

Figure 11. Time-division fracture distribution for the PF-GUN fracturing in well HG 79. The fractures formed by PF-GUN have an obvious guiding effect on the fracture extension of hydraulic fracturing. The fractures formed within 120 min of hydraulic fracturing are sliced according to time series, and the slice time is marked on the upper right corner of each panel. The yellow dots represent the microseismic events, and the green lines indicate the direction and scale of fractures. It is clear that the fracture scale and influence area increase gradually over time.

Table 5. Fracture Parameter Statistics for the 10 Test Wells

		fracturing induced fractures						
		main fracture						
well no.	fracture presetting technique	direction	east flank	west limb	branch fracture 1	branch fracture 2	branch fracture 3	branch fracture 4
HG 78	no treatment	nearly EW	232.1°	133°	NE43°			
HG 79	PF-GUN	NE80°	230.1°	213.6°	NW78°	NW80°		
HG 95		NE63°	232.1°	192.5°	NE60°	NW70°		
HG 173		NE65°	231°	172.7°	NE70°	NW56°		
HG 85	CO_2 blasting	NE48°	228.8°	211.7°	NE64°	nearly EW		
HG 83		NW50°	210°	211.7°	NW76°	nearly EW	nearly EW	
HG 86		NE50°	209.7°	214.2°	NE56°	nearly EW	nearly EW	
HG 87		NE40°	231°	212.5°	NW35°	NW75°	nearly EW	
HG 82		NE60°	231.1°	212.5°	NE40°	NE75°	NW60°	NW80°
HG 88		NE50°	211.2°	213.6°	NE45°	nearly EW	nearly EW	nearly EW

wells in the test area. The results show that compared with well HG 78 (without preset fractures), more than 1 branch fracture was generated in each of the nine test wells after large-scale hydraulic fracturing was conducted, and the intersection angle of multiple fractures was large, with an average of 60−120°. After using the PF-GUN fracture preset, one main fracture and two branch fractures were formed in three wells of hydraulic fracturing. Six wells using the CO_2 blasting preset formed two or more branch fractures, three wells of which formed three branch fractures and two wells formed four branch fractures. Wang et al.[56] believed that the mechanism of CO_2 blasting includes two aspects: there is a rapid formation of multiple radial fractures by the transmission of body waves, and then the quasi-static pressure formed by gas expansion causes the fractures to expand. Through laboratory testing and simulation methods, it is found that the length of the body-wave-generated radial fractures usually does not penetrate outward any farther than several borehole radii; later, quasi-static action will cause the propagation of about 4 fractures. The results are consistent with microseismic monitoring of the number of fractures formed by hydraulic fracturing after CO_2 blasting preset. According to microseismic monitoring results, the radial fracture length formed by quasi-static action can reach 20 m.

According to Cao et al.,[57] CO_2 blasting technology can form radial fractures from centimeters to meters scales in coal reservoirs. Blasting loading experiments of anthracite samples under a CO_2 overpressure of 21755 psi (150 MPa) were carried out, and a field emission scanning electron microscope (FESEM) was used to quantify coal matrix damage. Figure 12 shows the results; the CO_2 gas beam first destroys the fracture system, and the CO_2 gas jet produces a damage mark (DM) on the coal matrix, resulting in the tensile deformation of the matrix. Then, the three fractures start from DM and extend radially to different directions, inducing a triradial-wing (TRW) fracture pattern. When numerical trifractures are connected and form a complex fracture network, a three-dimensional fracture network is formed. The results also prove

https://doi.org/10.1021/acsomega.2c07001
ACS Omega 2023, 8, 6584−6596

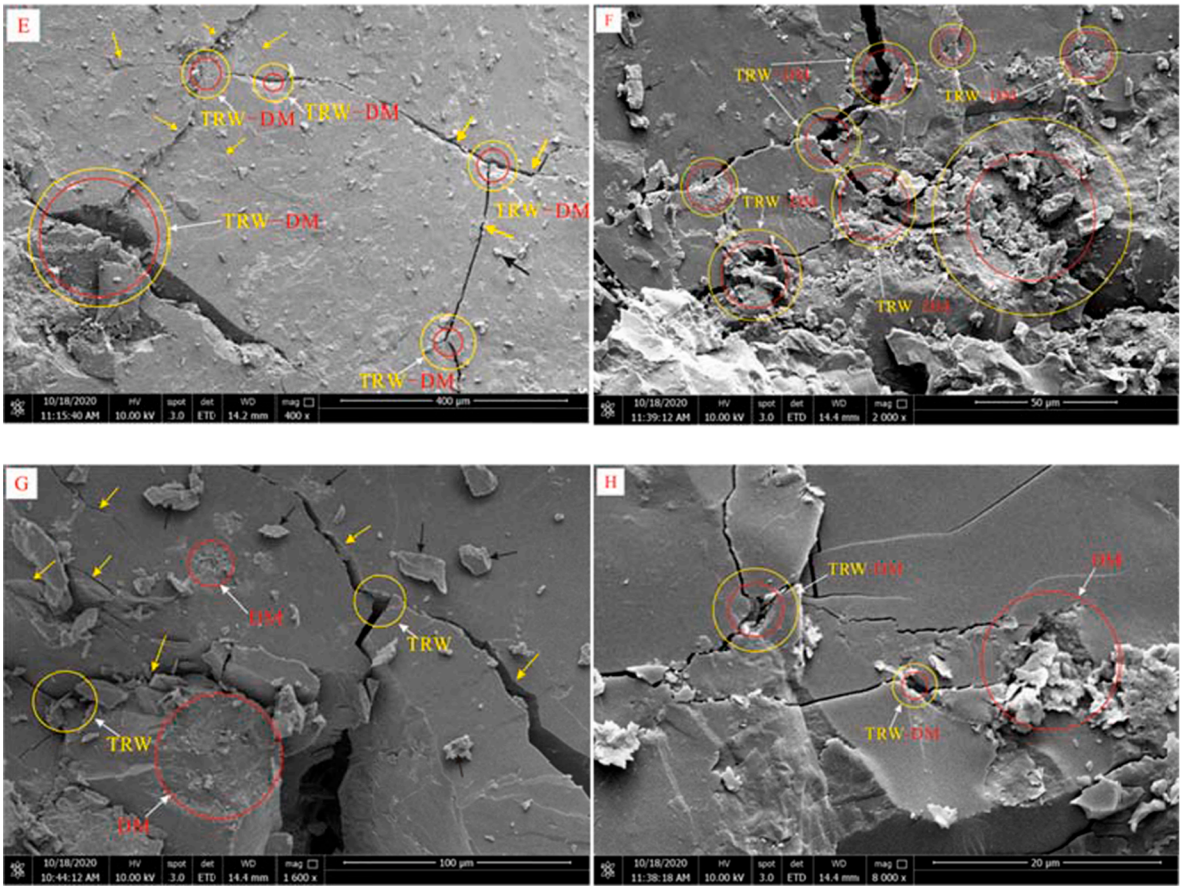

Figure 12. (E−H) SEM photos of microfractures in CO_2 dynamically impacted coal at different positions of coal samples.[57] Adapted with permission from ref 57. There are two typical geological phenomena in the SEM photos; one is the damage mark (DM) which is marked with a red circle, and the other is the triradial-wing (TRW) fracture which is marked with a yellow circle. The multifracture phenomenon under microscopic conditions is exactly consistent with the large-scale fractures revealed by microseismic monitoring.

that, after CO_2 blasting, the impact load of CO_2 forms three branched radial fractures in the coal matrix, which is consistent with the results of microseismic monitoring.

Overall, the number of branch fractures induced via hydraulic fracturing in the six wells in which the CO_2 blasting fracture presetting technique was used was greater than the number of branch fractures induced using the PF-GUN fracture presetting technique. The angle between the branch fractures and the main fracture produced via hydraulic fracturing after CO_2 blasting fracture presetting was greater than that for the PF-GUN fracture presetting technique. Therefore, from the perspective of the morphological distribution of the fractures, the presetting of CO_2 blasting fractures to form complex multiple fractures was better than that achieved using the PF-GUN fracture presetting technique.

3.2.2. Effect of Multifracturing on CBM Production. Production data from the experimental wells were collected and analyzed in detail. The maximum daily production of the nine multifractured wells was 1228.8 m^3/d (well HG 83) (Figure 13), and the maximum average daily production was 529.9 m^3/d (Table 6). The average daily production increased by 51.4% after multifracturing compared to the region's previous average production of 350 m^3/d.

After 1 year of drainage, the total production of wells HG 83 and HG 86 exceeded 100000 m^3. The production of the six well fractures using the CO_2 blasting fracture presetting technique was generally higher than that of the three wells

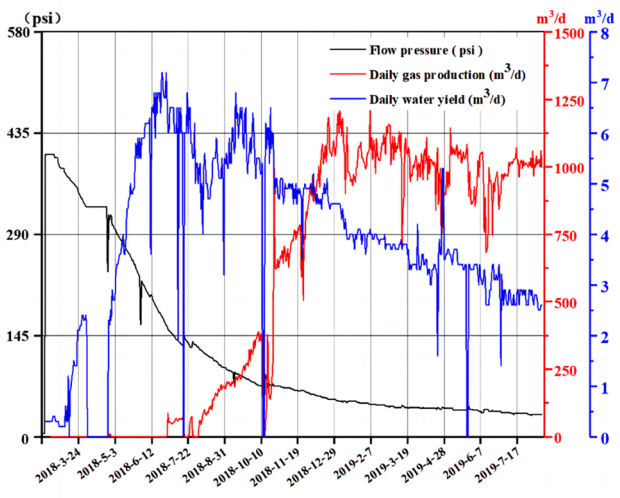

Figure 13. Production curve of well HG 83.

fractured using the PF-GUN fracture presetting technique. This further illustrates the advantage of using the CO_2 blasting fracture presetting technique in low-permeability reservoirs.

3.3. Discussion of Multifracturing of Coal Reservoirs. *3.3.1. Multifracturing Mechanisms of CO_2 Blasting and PF-GUN.* Numerous previous studies have been conducted on the mechanism of fracture formation in inorganic rocks induced by

https://doi.org/10.1021/acsomega.2c07001
ACS Omega 2023, 8, 6584−6596

Table 6. Drainage Data Statistics for the 10 Multifractured Demonstration Wells (Data as of February 20, 2019)

well no.	opening pumping pressure (psi)	critical desorption pressure (psi)	flow pressure (psi)	case pressure (psi)	maximum daily gas production (m^3/d)	maximum daily water yield (m^3/d)	cumulative gas production (m^3)	total water (m^3)
HG 78	350.99	153.74	36.26	14.50	298.5	5.9	39807.4	337.6
HG 79	324.88	147.94	11.60	7.25	97.1	4.6	11052.2	887.0
HG 82	359.69	221.91	30.46	20.31	535	3.96	83402.1	631.3
HG 83	404.66	152.29	44.96	31.91	1228.8	7.2	129364.2	1551.5
HG 85	381.45	174.05	31.91	10.15	945	4.18	59911.1	778.3
HG 86	417.71	126.18	30.46	21.76	821.8	4.8	105702.7	558.5
HG 87	314.73	139.24	21.76	13.05	187.7	6.48	22628.3	879.9
HG 88	327.79	113.13	13.05	0.00	179.4	1.93	16635.9	448.0
HG 95	380.00	124.73	27.56	7.25	284.3	6.1	29159.2	740.1
HG 173	234.96	89.92	36.26	21.76	483.2	12.2	43481.6	2405.7

high-pressure gas. Cuderman et al.[58,59] conducted in-depth research on the behavior characteristics of fractures under the action of high-energy gas and determined that the relationship between the pressurization time of the radial fractures produced by high-energy gas fracturing is

$$\frac{\pi D}{2C_R} < t_m < \frac{8\pi D}{C_R} \quad (1)$$

where t_m is the blasting time to the peak pressure (s), D is the borehole (m), and C_R is the Rayleigh surface wave velocity (m/s).

The Rayleigh surface wave velocity of the No. 3 coal seam in the Shanxi Formation in the Lu'an mining area is 1590 m/s, and the diameter of the completion casing of all of the test wells is 139.7 mm. Using eq 1, the best pressurization time for the formation of radial fractures using high-energy gas in the coal reservoirs in this area was calculated to be 0.2−3.0 ms (Figure 14).

We tested the impact pressure of CO_2 blasting in the laboratory, and the pressure temporal curves are shown in Figure 15a.

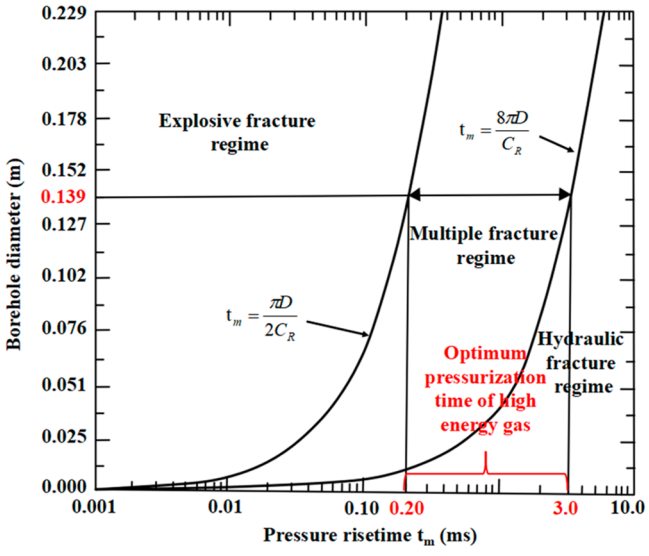

Figure 14. Relationship between the fracture morphology and pressurization time.[59] Reprinted in part with permission from ref 59. Multifracturing has strict requirements on the pressurization time of fracturing load. Under the condition of 139.7 mm wellbore diameter, the optimum pressurization time of multifracturing is 0.2−3.0 ms.

The main factors affecting the effect of the dynamic load fracture presetting using high-pressure gas are the pressurization rate, pressure peak, and peak duration. The first wave peak characteristics of the pressure−time history of the high-pressure gas play a decisive role in the effect of the fracturing of the coal seam. Using MATLAB software, the pressure data for the first peak of the CO_2 blasting were fitted numerically. The fitting function obtained under the condition of 95% confidence is

$$CO_2 \text{ blasting: } p(t) = 26498.3te^{-0.4874t} \quad (2)$$

According to eq 2, the pressurization rate of the CO_2 blasting was 26498.3 psi/ms, and the time required for the pressure to increase to the highest peak was 2.05 ms. Based on actual test data compiled from the literature,[41,42] the pressurization rate of the PF-GUN is 29−72.5 psi/ms, and the time required for the pressure to increase to the highest peak is 200 ms (Figure 15b). Based on the theoretical calculations, it was concluded that the CO_2 blasting technique was more consistent with the use of high-energy gas to fracture the coal seams in the study area and to form multiple fractures in the best pressurization time range of 0.2−3 ms.

3.3.2. Advantages of CO_2 Blasting in Enhancing CBM Drainage Effectiveness. The core technical principle of CO_2 blasting is that the high-pressure gas forms long fractures and large-scale fracture pressure relief rings in the coal seam. CO_2 blasting has three unique advantages. First, CO_2 blasting is a low-detonation-velocity and high-pressure gas fracturing technique; thus, it is more conducive to the formation of long fractures and large-scale fracture circles. The high-pressure gas propagation speed of the CO_2 blasting technique is 300−400 m/s, which is one tenth of the high-pressure gas propagation speed of explosive blasting (3000−4000 m/s). This low-speed propagation is more conducive to the formation of long fractures. Second, CO_2 blasting has a pressurization rate that is more compatible with the characteristics of coal reservoirs, and it has the essential advantage of forming radial fractures in coal reservoirs. Third, the CO_2 blasting pressure is relatively low, and there is no ultrahigh pressure shock wave; thus, a coal crushing compaction zone does not form near the hole wall, and only a large-scale fracture circle is formed.

In addition, the role of CO_2 blasting in a coal seam is not only the stress wave damage produced in the front-end high-pressure gas phase jet stage but also the later quasi-static high-pressure gas-phase expansion to reactivate the pre-existing fracture system. In general, the greater the total amount of CO_2

https://doi.org/10.1021/acsomega.2c07001
ACS Omega 2023, 8, 6584−6596

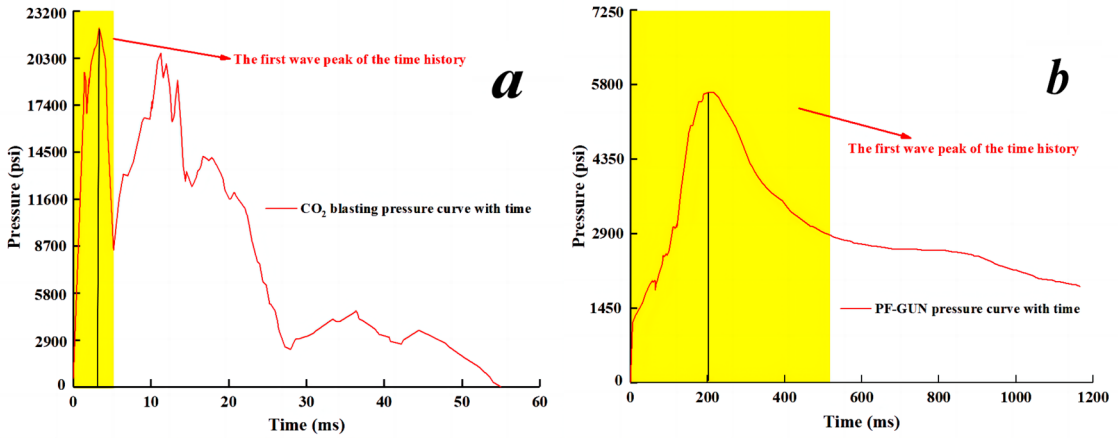

Figure 15. (a) Pressure temporal curves of CO_2 blasting. (b) Pressure temporal curves of PF-GUN. The numerical fitting method was used to fit the pressurization times of two dynamic fracturing loads; that of CO_2 blasting is 2.05 ms, and that of PF-GUN is 200 ms.

gas used in a single well, the longer the quasi-static duration of the high-pressure gas phase, which is more conducive to the formation of long fractures and large-volume retensioning fractures. However, the complex fracture system in a coal reservoir has a serious filtration effect on the fluid. Since the new fracture system formed via CO_2 blasting expands to a certain distance, when the filtration amount is greater than the total amount of gas, the fracture stops extending and instead disperses in the coal seam.

The relationship between the consumption of CO_2 in a single well and the fracture extension scale in six wells (CO_2 blasting test) revealed that, as the CO_2 consumption increases, the scale of the fracture propagation initially increases and then decreases (Figure 16). This indicates that, in a reservoir with a

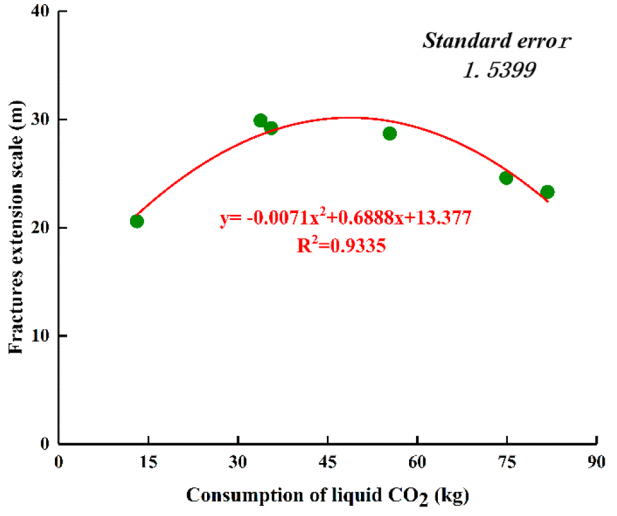

Figure 16. Relationship of fracture scale and liquid CO_2 consumption in a single well.

certain permeability, the CO_2 blasting multifracture fracturing technique has a maximum fracture length, and simply increasing the single-well CO_2 usage cannot increase the fracture extension length. This phenomenon is the result of CO_2 blasting pressure, CO_2 capacity, and coal reservoir properties. On the one hand, blasting forms a stress wave, causing coal seam cracking. On the other hand, CO_2 gas pulses through fractures and extends the pre-existing fracture system. However, the coal seam is a multifracture reservoir with a large filtration coefficient; the fracture will not extend after reaching the maximum scale under a certain gas displacement condition. When the consumption of CO_2 used is continuously increased in the later stage, the coal matrix expands due to the strong adsorption of CO_2, causing the existing cracks to close and the scale of crack propagation to decrease. This provides a research direction for further optimization of the CO_2 blasting technique.

4. CONCLUSIONS

In the study area, two dynamic load fracturing techniques, CO_2 blasting and PF-GUN, were compared. The effect of multifracturing was analyzed via microseismic monitoring and performance of gas production. The following conclusions can be drawn

(1) Both CO_2 blasting and PF-GUN dynamic loads have multifracture effects in coal reservoirs. The number of fractures formed via CO_2 blasting is larger, the morphology is more complex, and the intersection angle of the new fractures is larger, but the extension distance is relatively short.

(2) The radial fractures formed via CO_2 blasting in the near-wellbore zone has an obvious guiding effect on large-scale hydraulic fracturing. The extension direction of a fracture formed by the combination of the two does not completely align with the direction of the maximum principal stress, and it has typical multifracture characteristics.

(3) CO_2 blasting shows a good application effect in low-permeability CBM development. The stress wave produced by CO_2 blasting has the typical characteristics of low frequency and long wavelength, which may be potential advantages to form large-scale fractures. This is the fundamental mechanism of multifracturing by dynamic loads and should be the focus of future research.

AUTHOR INFORMATION

Corresponding Author

Lin Tian − *Institute of Resources & Environment, Henan Polytechnic University, Jiaozuo 454000, People's Republic of China; Gas Geology and Engineering Research Center,*

https://doi.org/10.1021/acsomega.2c07001
ACS Omega 2023, 8, 6584−6596

Henan Polytechnic University, Jiaozuo 454000, People's Republic of China; orcid.org/0000-0002-1306-2038; Phone: +86 0391 398-6982; Email: tillit6563@126.com

Authors

Yufei Qi − *Institute of Resources & Environment, Henan Polytechnic University, Jiaozuo 454000, People's Republic of China; Gas Geology and Engineering Research Center, Henan Polytechnic University, Jiaozuo 454000, People's Republic of China*

Yunxing Cao − *Institute of Resources & Environment, Henan Polytechnic University, Jiaozuo 454000, People's Republic of China; Gas Geology and Engineering Research Center, Collaborative Innovation Center of Coalbed Methane and Shale Gas for Central Plains Economic Region, Henan Province, and Henan International Joint Laboratory for Unconventional Energy Geology and Development, Henan Polytechnic University, Jiaozuo 454000, People's Republic of China; Collaborative Innovation Center of Coal Work Safety and Clean High Efficiency Utilization, Henan Polytechnic University, Jiaozuo 454000, People's Republic of China*

Jinghao Wu − *Institute of Resources & Environment, Henan Polytechnic University, Jiaozuo 454000, People's Republic of China; Henan International Joint Laboratory for Unconventional Energy Geology and Development, Henan Polytechnic University, Jiaozuo 454000, People's Republic of China*

Junsheng Zhang − *Institute of Resources & Environment, Henan Polytechnic University, Jiaozuo 454000, People's Republic of China; Henan International Joint Laboratory for Unconventional Energy Geology and Development, Henan Polytechnic University, Jiaozuo 454000, People's Republic of China*

Yongxing Cao − *Henan Ark New Energy Co., Ltd, Jiaozuo 454000, People's Republic of China*

Baoku Cui − *Lu'an Chemical Group Co., Led., Changzhi 046200, People's Republic of China*

Complete contact information is available at: https://pubs.acs.org/10.1021/acsomega.2c07001

Author Contributions

Y.Q.: methodology, data analysis, chart drawing, writing - original draft and editing. L.T.: methodology, conceptualization, project administration, supervision, writing - review and editing. Y.C.: conceptualization, funding acquisition, supervision, methodology. J.W.: conceptualization, data analysis, chart drawing. J.Z.: conceptualization, data analysis. Y.C.: field engineering test. B.C.: field engineering test.

Notes

The authors declare no competing financial interest.

■ ACKNOWLEDGMENTS

This research was funded by the National Natural Science Foundation of China (grant no. 42230814) and the Scientific and Technological Project of Henan Province (grant no. 222102320090).

■ REFERENCES

(1) Jiang, C. B.; Wang, Y. F.; Duan, M. K.; Guo, X. W.; Chen, Y. F.; Yang, Y. Experimental study on the evolution of pore-fracture structures and mechanism of permeability enhancement in coal under cyclic thermal shock. *Fuel.* **2021**, *304*, 121455.

(2) Mou, P. W.; Pan, J. N.; Wang, K.; Wei, J.; Yang, Y. H.; Wang, X. L. Influences of hydraulic fracturing on microfractures of high-rank coal under different in-situ stress conditions. *Fuel.* **2021**, *287*, 119566.

(3) Wang, X. L.; Pan, J. N.; Wang, K.; Mou, P. W.; Li, J. X. Fracture variation in high-rank coal induced by hydraulic fracturing using X-ray computer tomography and digital volume correlation. *International Journal of Coal Geology.* **2022**, *252*, 103942.

(4) Nguyen-Le, V.; Shin, H. Artificial neural network prediction models for Montney shale gas production profile based on reservoir and fracture network parameters. *Energy.* **2022**, *244*, 123150.

(5) Zeng, F. H.; Zhang, T.; Guo, J. C. Shale gas mass transfer characteristics in hydration-induced fracture networks. *Journal of Natural Gas Science and Engineering.* **2022**, *107*, 104767.

(6) Yang, Q.; Li, B.; Shao, M. R.; Zhang, H. J. Production performance of perforation clusters during multistage fracturing in shale gas reservoirs. *Acs Omega.* **2021**, *6* (40), 26231−26238.

(7) Zhao, Z. H.; Zheng, Y. C.; Zeng, B.; Song, Y. Investigation and application of high-efficiency network fracturing technology for deep shale gas in the southern sichuan basin. *Acs Omega.* **2022**, *7* (16), 14276−14282.

(8) Lei, Q.; et al. Progress and prospects of horizontal well fracturing technology for shale oil and gas reservoirs. *Petroleum Exploration and Development.* **2022**, *49* (1), 191−199.

(9) Liu, J. H.; Lu, M. J.; Sheng, G. L. Description of fracture network of hydraulic fracturing vertical wells in unconventional reservoirs. *Frontiers in Earth Science.* **2021**, *9*, 749181.

(10) Chen, B.; Barboza, B. R.; Sun, Y. N.; Bai, J.; Thomas, H. R.; Dutko, M.; Cottrell, M.; Li, C. F. A review of hydraulic fracturing simulation. *Archives of Computational Methods in Engineering.* **2022**, *29* (4), 1−58.

(11) Yu, W.; Luo, Z.; Javadpour, F.; Varavei, A.; Sepehrnoori, K. Sensitivity analysis of hydraulic fracture geometry in shale gas reservoirs. *Journal of Petroleum Science and Engineering.* **2014**, *113*, 1−7.

(12) Chen, M.; Guo, T. K.; Xu, Y.; Qu, Z. Q.; Zhang, S. H.; Zhou, T.; Wang, Y. P. Evolution mechanism of optical fiber strain induced by multi-fracture growth during fracturing in horizontal wells. *Petroleum Exploration and Development.* **2022**, *49* (1), 211−222.

(13) Hou, X. J.; Zhang, X. H.; Guo, B. Y. Mathematical modeling of fluid flow to unconventional oil wells with radial fractures and its testing with field data. *Journal of Energy Resources Technology.* **2019**, *141* (7), 070702.

(14) Tu, Z. Y.; Hu, X. D.; Zhou, F. J.; Huang, G. P.; Han, S. B.; Zhou, Q. L. A new multi-fracture geometry inversion model based on hydraulic-fracture treatment pressure falloff data. *Journal of Petroleum Science and Engineering.* **2022**, *215*, 110724.

(15) Li, Z. Q.; Qi, Z. L.; Yan, W. D.; Huang, X. L.; Xiao, Q. H.; Mo, F.; Fang, F. F. New algorithm to simulate fracture network propagation using stationary and moving coordinates in naturally fractured reservoirs. *Energy Science & Engineering.* **2020**, *8* (11), 4025−4042.

(16) Hu, Y. Q.; Jia, S. G.; Zhao, J. Z.; Zhang, Y.; Mi, Q. B. Study on control conditions of fracture network fracturing. *Journal of Southwest Petroleum University(Science & Technology Edition).* **2013**, *35* (04), 126−132. (in Chinese)

(17) Cho, S. H.; Nakamura, Y.; Kaneko, K. Dynamic fracture process analysis of rock subjected to a stress wave and gas pressurization. *International Journal of Rock Mechanics and Mining Sciences.* **2004**, *41* (3), 439−439.

(18) Luo, Z. M. Quantitative analysis of multi-fracture interference in fractured wells. *Natural Gas Exploration and Development.* **2008**, *31* (04), 37−40. (in Chinese)

(19) Li, J.; Cao, L. Y.; Guo, B. Y.; Zhang, X. H. Prediction of productivity of high energy gas-fractured oil wells. *Petroleum Science and Engineering.* **2018**, *160*, 510−518.

(20) Pu, J. Y.; Yang, Y.; Pu, C. S.; Zou, H. J. On some studies about the dynamic mechanisms of carbon monoxide flow and diffusion during high energy gas fracturing. *Safety science.* **2012**, *50* (4), 903−908.

(21) Pu, C. S.; Rao, P.; Zhou, M.; Wu, F. P.; Qin, W. L. On studies of formation, diffusion mechanisms and prevention measures of CO during HEGF in low permeability oil reservoirs. *Journal of Hydrodynamics.* **2010**, *22* (5), 387−392.
(22) Guo, B. Y.; Shan, J.; Feng, Y. Productivity of blast-fractured wells in liquid-rich shale gas formations. *Journal of Natural Gas Science and Engineering.* **2014**, *18*, 360−367.
(23) Wu, F. P.; Ding, Q. S.; Shi, X. J.; Tan, X. Y. The transient intrusion effect of high energy fluid on the rock failure around the wellbore during the dynamic stimulation process. *Engineering Fracture Mechanics.* **2020**, *239*, 107294.
(24) Al-Nakhli, A.; Tariq, Z.; Mahmoud, M.; Abdulraheem, A. Thermochemical-Pulse Fracturing of Tight Gas: Investigation of Pulse Loading on Fracturing Behavior. In *SPE/IADC Middle East Drilling Technology Conference and Exhibition*; OnePetro: 2021.
(25) Tariq, Z.; Mahmoud, M.; Abdulraheem, A.; Al-Nakhli, A.; Bataweel, M. A review of pulse fracturing treatment: an emerging stimulation technique for unconventional reservoirs. In *SPE Middle East Oil and Gas Show and Conference*; OnePetro: 2019.
(26) Tariq, Z.; Mahmoud, M.; Abdulraheem, A.; Al-Nakhli, A.; BaTaweel, M. An experimental study to reduce the fracture pressure of high strength rocks using a novel thermochemical fracturing approach. *Geofluids* **2019**, *2019*, 1−16.
(27) Al-Nakhli, A.; Zeeshan, T.; Mahmoud, M.; Abdulraheem, A. Reducing breakdown pressure of tight reservoirs via in-situ pulses: impact of mineralogy. In *SPE/IATMI Asia Pacific Oil & Gas Conference and Exhibition*; OnePetro: 2020.
(28) Tariq, Z.; Mahmoud, M.; Abdulraheem, A.; Al-Nakhli, A.; BaTaweel, M. An experimental study to reduce the breakdown pressure of the unconventional carbonate rock by cyclic injection of thermochemical fluids. *Journal of Petroleum Science and Engineering.* **2020**, *187*, 106859.
(29) Al-Nakhli, A.; Tariq, Z.; Mahmoud, M.; Abdulraheem, A. A state-of-the-art technology to reduce fracturing pressure in tight gas formations using thermochemical pulse. In *Unconventional Resources Technology Conference*; 2020; pp 1177−1187.
(30) Al-Nakhli, A.; Tariq, Z.; Mahmoud, M.; Abdulraheem, A. Chemically-Induced Pressure Pulse: Fracturing Competent Reservoirs. In *SPE/IADC Middle East Drilling Technology Conference and Exhibition*; OnePetro: 2021.
(31) Tariq, Z.; Mahmoud, M.; Abdulraheem, A.; Al-Shehri, D.; Murtaza, M. An environment friendly approach to reduce the breakdown pressure of high strength unconventional rocks by cyclic hydraulic fracturing. *Journal of Energy Resources Technology.* **2020**, *142* (4), No. 043002.
(32) Kalam, S.; Afagwu, C.; Al Jaberi, J.; Siddig, O. M.; Tariq, Z.; Mahmoud, M.; Abdulraheem, A. A review on non-aqueous fracturing techniques in unconventional reservoirs. *Journal of Natural Gas Science and Engineering.* **2021**, *95*, 104223.
(33) Shi, B.; Cao, Y. X.; Tian, L.; Zhang, J. S.; Liu, S. M. CO_2 Gas Fracturing in High Dip Angled Coal Seams for Improved Gas Drainage Efficiency at Hashatu Coal Mine. *Energy & Fuels.* **2022**, *36* (5), 2763−2774.
(34) Fan, Y.; Qin, B.; Zhou, Q.; Shi, Q.; Ma, D.; Wu, J. Liquid CO_2 phase transition fracturing technology and its application in enhancing gas drainage of coal mines. *Adsorption Science & Technology.* **2020**, *38* (9-10), 393−412.
(35) Shang, Z.; Wang, H. F.; Li, B.; Cheng, Y. P.; Zhang, X. H.; Zhao, F.; Zhang, X.; Hao, C. M.; Wang, Z. Y. Fracture processes in coal measures strata under liquid CO_2 phase transition blasting. *Engineering Fracture Mechanics.* **2021**, *254*, 107902.
(36) Wang, H. D.; Cheng, Z. H.; Zou, Q. L.; Li, Z. H.; Sun, F. L.; Yang, H. W.; Lei, Y. Elimination of coal and gas outburst risk of an outburst-prone coal seam using controllable liquid CO_2 phase transition fracturing. *Fuel.* **2021**, *284*, 119091.
(37) Hu, G. Z.; He, W. R.; Sun, M. Enhancing coal seam gas using liquid CO_2 phase-transition blasting with cross-measure borehole. *Journal of Natural Gas Science and Engineering.* **2018**, *60*, 164−173.
(38) Cao, Y. X.; Zhang, J. S.; Zhai, H.; Fu, G. T.; Tian, L.; Liu, S. M. CO_2 gas fracturing: A novel reservoir stimulation technology in low permeability gassy coal seams. *Fuel.* **2017**, *203*, 197−207.
(39) Cao, Y. X.; Tian, L.; Fan, Y. C.; Liu, J. Z.; Zhang, S. Study on fracture circle morphology of CO_2 gas phase fracturing in low permeability coal seam. *Coal Science and Technology.* **2018**, *46* (06), 46−51. (in Chinese)
(40) Yang, B. G.; Zhang, J. S.; Linghu, J. S.; Cao, Y. X. CO_2 gas phase fracturing high efficiency extraction and outburst prevention technology in outburst coal seam. *Coal Geology & Exploration.* **2021**, *49* (03), 85−94. (in Chinese)
(41) Feng, G. F.; An, Z.; Wang, C. S.; Yao, Y. W.; Xie, M. Z. Application of long section pulse deflagration fracturing technology in N2−4-D48 well. *Oil Drilling & Production Technology.* **2012**, *34* (06), 77−79. (in Chinese)
(42) Wang, C. S.; Zhao, H. H.; Niu, Y. Y.; Wang, F.; Feng, W. D. Application of MP PF Gun Pulse Deflagration Fracturing Technology in Oman SSM-XX Well. *Engineering Blasting.* **2014**, *20* (06), 32−35. (in Chinese)
(43) Bai, Y.; Sun, L.; Wei, C. H. A coupled gas flow-mechanical damage model and its numerical simulations on high energy gas fracturing. *Geofluids.* **2020**, *2020*, 1−14.
(44) Tian, L.; Cao, Y. X.; Liu, S. M.; Shi, B.; Liu, J. Z.; Elsworth, D. Coalbed methane reservoir fracture evaluation through the novel passive microseismic survey and its implications on permeable and gas production. *Journal of Natural Gas Science and Engineering.* **2020**, *76*, 103181.
(45) Tian, L.; Li, Z. H.; Cao, Y. X.; Liu, S. M.; Song, Y. L. In situ stress distribution and variation monitored by microseismic tracking on a fractured horizontal well: a case study from the Qinshui basin. *Acs Omega.* **2022**, *7* (16), 14363−14370.
(46) Huang, S. P.; Liu, D. M.; Cai, Y. D.; Gan, Q. In situ stress distribution and its impact on CBM reservoir properties in the Zhengzhuang area, southern Qinshui Basin, North China. *Journal of Natural Gas Science and Engineering.* **2019**, *61*, 83−96.
(47) Luo, B.; Lellouch, A.; Jin, G.; Biondi, B.; Simmons, J. Seismic inversion of shale reservoir properties using microseismic-induced guided waves recorded by distributed acoustic sensing. *Geophysics.* **2021**, *86* (4), R383−R397.
(48) Jiang, Y. D.; Zhao, Y. X.; Wang, H. W.; Zhu, J. A review of mechanism and prevention technologies of coal bumps in China. *Journal of Rock Mechanics and Geotechnical Engineering.* **2017**, *9* (1), 180−194.
(49) Hu, Y. Q.; Li, Z. Q.; Zhao, J. Z.; Tao, Z. W.; Gao, P. Prediction and analysis of the stimulated reservoir volume for shale gas reservoirs based on rock failure mechanism. *Environmental Earth Sciences.* **2017**, *76* (15), 1−13.
(50) Fang, Y.; Elsworth, D.; Cladouhos, T. T. Reservoir permeability mapping using microearthquake data. *Geothermics.* **2018**, *72*, 83−100.
(51) Cheng, Y. G.; Lu, Y. Y.; Ge, Z. L.; Cheng, L.; Zheng, J. W.; Zhang, W. F. Experimental study on crack propagation control and mechanism analysis of directional hydraulic fracturing. *Fuel.* **2018**, *218*, 316−324.
(52) Zhou, D. S.; Zheng, P.; Peng, J.; He, P. Induced stress and interaction of fractures during hydraulic fracturing in shale formation. *Journal of Energy Resources Technology.* **2015**, *137* (6), No. 062902.
(53) Liu, J.; Yao, Y. B.; Liu, D. M.; Xu, L. L.; Elsworth, D.; Huang, S. P.; Luo, W. J. Experimental simulation of the hydraulic fracture propagation in an anthracite coal reservoir in the southern Qinshui basin, China. *Journal of Petroleum Science and Engineering.* **2018**, *168*, 400−408.
(54) Lu, W. Y.; Bai, E.; Wei, L.; He, C. C.; Sun, Y. H.; Shi, L. Numerical simulation on spatial steering rule of directional perforation hydraulic fractures in low-permeability reservoir. *Frontiers in Earth Science.* **2022**, *10*, 1007218.
(55) Zhang, B. H.; Ji, B. X.; Liu, W. F. The study on mechanics of hydraulic fracture propagation direction in shale and numerical simulation. *Geomechanics and Geophysics for Geo-Energy and Geo-Resources.* **2018**, *4* (2), 119−127.

https://doi.org/10.1021/acsomega.2c07001
ACS Omega 2023, 8, 6584−6596

(56) Wang, J. H.; Elsworth, D.; Cao, Y. X.; Liu, S. M. Reach and geometry of dynamic gas-driven fractures. *International Journal of Rock Mechanics and Mining Sciences.* **2020**, *129*, 104287.
(57) Cao, Y. X.; Zhang, J. S.; Zhang, X. S.; Liu, S. M.; Elsworth, D. Micro-fractures in coal induced by high pressure CO_2 gas fracturing. *Fuel.* **2022**, *311*, 122148.
(58) Wang, C. S.; Yao, Y. W.; Feng, G. F.; Yang, X. B.; Yuan, L. J. Application of pulse deflagration fracturing technology in coalbed methane well. *Drilling & Production Technology.* **2013**, *36* (02), 128−130. (in Chinese)
(59) Cuderman, J. F.; Northrop, D. A. A Propellant-Based Technology for Multiple Fracturing Wellbores to Enhance Gas Recovery: Application and Results in Devonian Shale. *SPE Production Engineering.* **1986**, *1* (2), 97−103.

https://doi.org/10.1021/acsomega.2c07001
ACS Omega 2023, 8, 6584−6596